Phys. Lett. B 856 (2024) 138887

Contents lists available at ScienceDirect

Physics Letters B

journal homepage: www.elsevier.com/locate/physletb

Letter

Method for measuring the charge radii of charged hyperons from the time-like region

Yong-Hui Lin [a,*], Feng-Kun Guo [b,c,d,*], Ulf-G. Meißner [a,e,f]

[a] Helmholtz-Institut für Strahlen- und Kernphysik and Bethe Center for Theoretical Physics, Universität Bonn, D-53115 Bonn, Germany
[b] CAS Key Laboratory of Theoretical Physics, Institute of Theoretical Physics, Chinese Academy of Sciences, Beijing 100190, China
[c] School of Physical Sciences, University of Chinese Academy of Sciences, Beijing 100049, China
[d] Peng Huanwu Collaborative Center for Research and Education, Beihang University, Beijing 100191, China
[e] Institute for Advanced Simulation, Forschungszentrum Jülich, D-52425 Jülich, Germany
[f] Tbilisi State University, 0186 Tbilisi, Georgia

ARTICLE INFO

Editor: A. Ringwald

ABSTRACT

We propose a novel method for measuring the charge radii of charged stable hadrons, with which the first measurement of the charge radii of the Σ^+ and the Ξ^- is foreseen. The method explores the facts that the Dalitz decay $\psi(2S) \to Y\bar{Y}e^+e^-$ contains the hyperon form factors and the lowest measurable four-momentum transfer squared can be as low as $\sim 4m_e^2 = 1.05 \times 10^{-6}\,\text{GeV}^2$ in the time-like region. We identify a kinematic region where the hyperon form factors are essential and propose a method for subtracting the background from the data. It is estimated that the hyperon charge radii can be measured to a precision of about 0.2 fm with the BESIII experiment and one order of magnitude better at the future Super τ-Charm Facility. Moreover, the same method can be used to measure the charge radius of the proton, which provides an independent cross-check on the extraction of proton radius from elastic ep scattering or leptonic hydrogen spectroscopy.

1. Introduction

The size of a hadron, a consequence of the confinement of quarks and gluons inside a finite volume, is one of the most fundamental and simplest static properties. It is, however, not an unambiguously defined observable but depends on the probe used in experiments. The electric charge radius of a hadron defines its size seen by a photon probe and is encoded in its electromagnetic form factors (EMFFs). Systematic investigations of the hadron EMFFs from both theoretical and experimental perspectives have led to a better understanding of the internal structure of hadrons and the nonperturbative nature of quantum chromodynamics (QCD) at low energies. For recent reviews, see, e.g., Refs. [1–3].

Over the past decade, a remarkable surge in research dedicated to the nucleon EMFFs has been witnessed, which was spurred by the report of the first extraction of the proton charge radius from the spectroscopic measurement of muonic hydrogen with unprecedented precision in 2010 [4]. This value, 0.84184(67) fm [4,5], unexpectedly exhibited a 5σ deviation from the previously accepted one, 0.8768(69) fm [6], which was based on electron scattering and ordinary hydrogen spectroscopy measurements. Recently, a high-precision analysis, based on dispersion relations, of the world data of the nucleon EMFFs in the space- and time-like regions led to $r_E^p = 0.840(3)(4)\,\text{fm}$ [7], which fully agrees with the latest CODATA value, 0.8414(19) fm [8]. An important ingredient in this analysis is the isovector spectral function [9,10]. For reviews on the progress on the determination of the proton charge radius, we refer to [11–16].

It is important to highlight that the definition of the charge radius, $\langle (r_E^p)^2 \rangle = -6\, dG_E^p/dQ^2|_{Q^2=0}$, where G_E^p is the electric Sachs form factor of the proton, implies a greater sensitivity to the data at lower four-momentum transfer squared. This underscores the significance of measurements conducted at low momentum transfers in accurately determining the charge radius. Currently, the lowest accessible value of the four-momentum transfer squared for the proton charge radius extraction is reached by the PRad experiment, $Q^2 = 2.1 \times 10^{-4}\,\text{GeV}^2$ [17]. The follow-up program PRad-II under construction aims to reach values of Q^2 as low as $10^{-5}\,\text{GeV}^2$ [18].

While notable progress towards measuring the proton charge radius has been made in recent years, the experimental knowledge of the elec-

* Corresponding authors.
E-mail addresses: yonghui@hiskp.uni-bonn.de (Y.-H. Lin), fkguo@itp.ac.cn (F.-K. Guo), meissner@hiskp.uni-bonn.de (U.-G. Meißner).

https://doi.org/10.1016/j.physletb.2024.138887
Received 14 June 2024; Received in revised form 12 July 2024; Accepted 15 July 2024
Available online 18 July 2024

tromagnetic structure of other baryons and, in particular, of those with strangeness (the hyperons) is scarce due to absence of stable hyperon targets. So far, only the charge radius of the Σ^-, among all hyperons, has been measured to be 0.78(10) fm using a Σ^- beam at a mean energy of 610 GeV [19]. The fact that the kaon charge radius (0.560±0.031 fm) has been found to be smaller than that of the pion (0.659±0.004 fm) [20] suggests a flavor dependence of the hadron size [2,19,21,22]. There is also a large spread of theoretical predictions for the hyperon charge radii, covering the range from 0.6 to 1.0 fm for the Σ^+ and from 0.4 to 0.7 fm for Ξ^- [23–27]. To clarify how the hadron structure depends on the valence quark content and how the flavor SU(3) symmetry of QCD is broken, a systematic study of the charge radii of hyperons is necessary. Measurements of the hyperon and hyper-nucleus charge radii can also shed light on the baryon-baryon interactions; one particular example of this point is provided by the precise determination of $\langle(r_E^n)^2\rangle$ from the measurement of $\langle(r_E^d)^2\rangle - \langle(r_E^p)^2\rangle$ using the state-of-the-art nucleon-nucleon potentials [28], where the superscripts n and d denote neutron and deuteron, respectively. Additional interest on hyperons comes from the growing evidence that strange particles can have significant implications for astrophysics, such as the reduction of the maximum value of neutron star mass by the hyperon degrees of freedom [3,29].

In this Letter, we propose a novel method to determine the charge radii of charged hyperons, namely, to measure it in the time-like region in the four-body Dalitz decay $\psi(2S) \to Y\bar{Y}e^+e^-$, making use of the huge $\psi(2S)$ data sets, 2.7×10^9, collected at BESIII [30] and 6.4×10^{11} at the potential Super τ-Charm Facility (STCF) [31]. Here, Y denotes the Σ^+ and the Ξ^-. It opens an opportunity to access the hyperon EMFFs experimentally at an extremely low four-momentum transfer squared, i.e., $q^2 \equiv -Q^2 \sim 4m_e^2 = 1.05\times10^{-6}\,\text{GeV}^2$, since the electron and positron can be detected with a high efficiency as long as their transverse momenta are larger than a few tens of MeV (about 50 MeV at BESIII). The low $q^2 \simeq 4m_e^2$ can be reached by detecting the electron and positron produced with a small relative momentum. The resulting determination of the charge radii of charged hyperons will exhibit a high accuracy once sufficient events are collected. Furthermore, similar reactions with $Y\bar{Y}$ replaced by $p\bar{p}$ can be used to measure the proton charge radius, which provides an independent cross-check on the extraction of proton radius from elastic ep scattering or leptonic hydrogen spectroscopy, although the precision of this novel approach may not be competitive with that of existing high-accuracy measurements, such as the PRad experiment in ep scattering and the CREMA experiment in muonic hydrogen spectroscopy.

2. Dalitz decay $\psi(2S) \to Y\bar{Y}e^+e^-$

The considered Dalitz decay can happen through several mechanisms shown in Fig. 1, following the notation of Ref. [32]:

- type-X: $\psi(2S) \to \gamma^* X (X \to Y\bar{Y})$, see diagrams (a) and (b);
- type-A: $\psi(2S) \to \bar{Y} A (A \to \gamma^* Y)$, see diagram (c);
- type-B: $\psi(2S) \to Y B (B \to \gamma^* \bar{Y})$, see diagram (d).

In diagrams (a) and (b), the virtual photon is emitted from the charm or anti-charm quark in the $\psi(2S)$, and the $Y\bar{Y}$ pair is then mainly produced through two gluons. In diagrams (c) and (d), the $c\bar{c}$ pair first annihilates into three gluons (or one virtual photon) that hadronize into a hyperon-antihyperon pair, the virtual photon, which converts to e^+e^-, is emitted from the antihyperon or hyperon, respectively, via the final-state radiation (FSR), $\psi(2S) \to Y\bar{Y}\gamma^*_{\text{FSR}}(\gamma^*_{\text{FSR}} \to e^+e^-)$. The hyperon EMFFs are embodied in the decay amplitude of the type-A and type-B diagrams.

The differential rate of the decay process $\psi(2S) \to Y\bar{Y}e^+e^-$ can be written as

$$\frac{d\Gamma}{dm_{e^+e^-}dm_{Y\bar{Y}}d\cos\theta^* d\cos\theta' d\phi}$$

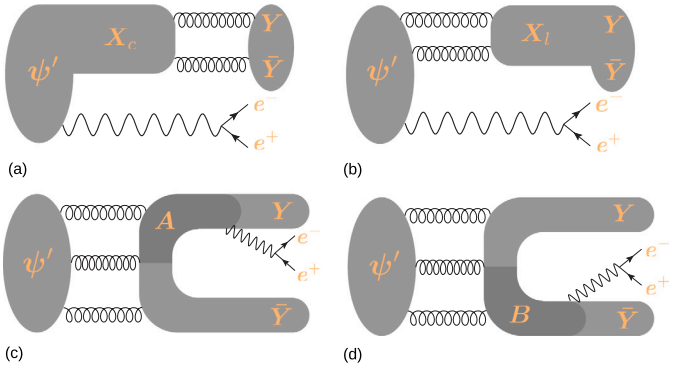

Fig. 1. Diagrams for the $\psi(2S) \to Y\bar{Y}e^+e^-$ process. The diagrams (a) and (b) are denoted as type-X, for which the $Y\bar{Y}$ pair is produced via two gluons, (c) as type-A and (d) as type-B, for which the light hadrons are produced via three gluons (or one virtual photon).

$$= \frac{|\vec{k}_{e^+e^-}||\vec{k}^*_Y||\vec{k}'_{e^-}|}{(2\pi)^6 16 M^2_{\psi(2S)}} \frac{C(q^2)}{3} \sum_{\text{spins}} |\mathcal{M}|^2, \tag{1}$$

where $\vec{k}_{e^+e^-}$, $\vec{k}^*_Y$ and $\vec{k}'_{e^-}$ are the three-momentum of e^+e^- in the $\psi(2S)$ rest frame, that of Y in the $Y\bar{Y}$ center-of-mass (c.m.) frame, and that of e^- in the e^+e^- c.m. frame, respectively. (θ^*, ϕ^*) and (θ', ϕ') parameterize the directions of three-momentum $\vec{k}^*_Y$ and $\vec{k}'_{e^-}$ in their respective center-of-mass frames. For the process under study, only one independent azimuthal angle is required, as illustrated in Fig. 2, and we adopt the convention $\phi' = \phi$ and $\phi^* = 0$. $C(q^2) \equiv y/(1-e^{-y})$ is the Sommerfeld-Gamow factor with $y \equiv \pi\alpha m_e/|\vec{k}'_{e^-}|$ and α the fine-structure constant, and

$$|\mathcal{M}|^2 = \left|\mathcal{M}_{\text{signal}}\right|^2 + \left|\mathcal{M}_X\right|^2, \tag{2}$$

$$\left|\mathcal{M}_{\text{signal}}\right|^2 \equiv \left|\mathcal{M}_{A+B}\right|^2 + 2\,\text{Re}\left(\mathcal{M}_{A+B}\mathcal{M}^*_X\right). \tag{3}$$

The decay $\psi(2S) \to Y_n\bar{Y}_n e^+e^-$, where Y_n denotes the neutral isospin partner of the charged hyperon Y, is dominated by the type-X diagrams since Y_n and $\bar{Y}_n$ are charge neutral.[1] Because the two-gluon exchange is isospin symmetric, the type-X contribution to the decay rate of $\psi(2S) \to Y\bar{Y}e^+e^-$ should equal to that of $\psi(2S) \to Y_n\bar{Y}_n e^+e^-$ up to tiny corrections. Therefore, the contribution from $\left|\mathcal{M}_X\right|^2$ in Eq. (2) to the differential decay rate of $\psi(2S) \to Y\bar{Y}e^+e^-$ can be eliminated by subtracting the differential decay rate of $\psi(2S) \to Y_n\bar{Y}_n e^+e^-$ from that of $\psi(2S) \to Y\bar{Y}e^+e^-$ (since both charged and neutral Σ and Ξ hyperons can be reconstructed from proton, π^- and photon(s), they can be easily detected). Then the hyperon EMFFs are contained in all the left terms, denoted as $\left|\mathcal{M}_{\text{signal}}\right|^2$, in the decay rate after subtraction.

However, not only the hyperon EMFFs but also the transition form factors from excited resonances to $\gamma^*Y/\bar{Y}$ can contribute to diagrams (c) and (d). Therefore, it is crucial to identify a kinematic region where the ground state octet hyperon contribution dominates over such background. When the $Y\bar{Y}$ invariant mass $m_{Y\bar{Y}}$ is large, the energy-momentum conservation forces both $m_{Y\gamma^*}$ and $m_{\bar{Y}\gamma^*}$ to be small, and thus the hyperon/anti-hyperon pole should dominate the type-A and type-B amplitudes. In the subsequent analysis, we will show that this is indeed the case. Given that the $\Sigma(1385)^+$ and $\Xi(1530)^-$ are the lowest-lying resonance that can couple to $\Sigma^+\gamma^*$ and $\Xi^-\gamma^*$, respectively, we investigate the $\Sigma(1385)^+$ and $\Xi(1530)^-$ contributions to pinpoint the

[1] Due to charge neutrality, the leading coupling of Y_n to the photon vanishes. The EMFF of the neutral hyperon starts from the mean square charge radius term, and is thus much smaller than that of the charged hyperon in the small Q^2 region. When precise data become available, such contributions can, in principle, be included in the analysis.

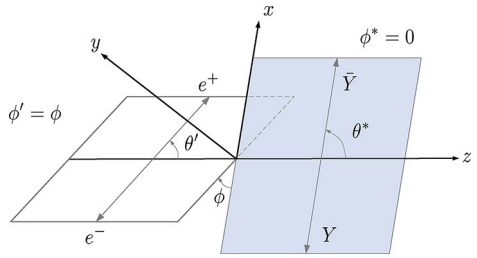

Fig. 2. Kinematics for the $\psi(2S) \to Y\bar{Y}e^+e^-$ process.

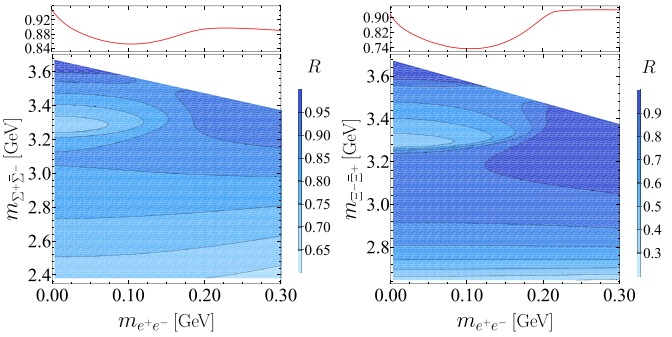

Fig. 3. Differential ratio R defined in Eq. (4) for Σ^+ (left) and Ξ^-. The projected subplots show the corresponding ratio with $m_{\Sigma^+\bar{\Sigma}^-}$ and $m_{\Xi^-\bar{\Xi}^+}$ integrated out from 2.8 and 2.9 GeV, respectively.

kinematic regions dominated by the Σ^+ and Ξ^- poles, respectively. We define the following differential ratio

$$\frac{dR}{dm_{e^+e^-}dm_{Y\bar{Y}}} = \frac{\int d\cos\theta^* d\cos\theta' d\phi\, d\Gamma^{Y}_{A+B}}{\int d\cos\theta^* d\cos\theta' d\phi\, d\Gamma^{Y+Y^*}_{A+B}}\,. \tag{4}$$

The amplitude of $\psi(2S)(p_0) \to e^-(p_1) + e^+(p_2) + Y(p_3) + \bar{Y}(p_4)$ can be written as,

$$i\mathcal{M}_{(i)} = H^{\mu}_{(i)} L^{\nu} \frac{-ig_{\mu\nu}}{q^2}, \tag{5}$$

where $q = p_0 - p_3 - p_4$ the four-momentum of the virtual photon, (i) =(a), (b), (c) or (d) refers to the corresponding diagram in Fig. 1, and the whole decay amplitude is decomposed into a hadronic (H^{μ}) and a leptonic (L^{ν}) contribution. The leptonic operator is given by

$$L^{\nu} = -ie\bar{u}_{s_{e^-}}(p_1)\gamma^{\nu} v_{s_{e^+}}(p_2)\,. \tag{6}$$

The EMFFs are contained in the hadronic operators, for which the vertices $\psi(2S)Y\bar{Y}$, $\psi(2S)Y^*\bar{Y}$ and $\psi(2S)Y\bar{Y}^*$ are constructed within the orbital-spin partial-wave framework, incorporating both S- and D-wave contributions [33–35]. The γY^*Y interaction is parameterized with a magnetic dipole form factor $g_M^{Y^*}$ normalized to the partial width of $Y^* \to Y + \gamma$ [36], and the electric quadrupole and Coulomb quadrupole terms have been neglected as they were found to be at the percent level for the analogous $\Delta \to N\gamma^*$ [37,38]. Technical details, including gauge invariance and off-shell effects [39–41], are provided in the Supplemental Material [42].

Using the dipole hypothesis for the elastic hyperon EMFFs and setting the charge radius to 0.8 fm, in the ballpark of the proton and Σ^- radii, we present the resulting ratio R, as defined in Eq. (4), in Fig. 3 for Σ^+ and Ξ^- hyperons. It is shown that for $m_{\Sigma^+\bar{\Sigma}^-} > 2.8\,\text{GeV}$ ($m_{\Xi^-\bar{\Xi}^+} > 2.9\,\text{GeV}$), the Σ^+ (Ξ^-) pole contributes at least 85% (74%) to the type-A and type-B mechanisms, which is similar with the proton case where there are no any visible $m_{p\gamma}$ or $m_{\bar{p}\gamma}$ bands in the Dalitz plot of $J/\psi \to p\bar{p}\gamma$ [32]. We checked that this ratio is insensitive to the input hyperon charge radius.

Therefore, it is feasible to extract the Σ^+ and Ξ^- EMFFs from the kinematic region of $m_{\Sigma^+\bar{\Sigma}^-} > 2.8\,\text{GeV}$ of the decay $\psi(2S) \to \Sigma^+\bar{\Sigma}^-e^+e^-$ and $m_{\Xi^-\bar{\Xi}^+} > 2.9\,\text{GeV}$ of the decay $\psi(2S) \to \Xi^-\bar{\Xi}^+e^+e^-$, respectively. The process can be measured at BESIII and at the potential STCF with two-orders-of-magnitude more events. One notable advantage is the ability to reach an unprecedented low momentum transfer squared ($4m_e^2$) through this decay, which offers a way for measuring of the unknown charge radii of the Σ^+ and Ξ^-.

3. Sensitivity to the charge radii of Σ^+ and Ξ^-

By subtracting the type-X contribution using the $\Sigma^0\bar{\Sigma}^0$ and $\Xi^0\bar{\Xi}^0$ measurements, as discussed above, and employing a parameterization for the elastic EMFFs of Σ^+ and Ξ^-, the differential decay rates, obtained within the previously described formalism, can be fitted to the event distribution in the low $m^2_{e^+e^-}$ region to extract the shape parameters of Σ^+ and Ξ^- hyperons, respectively. It is instructive to investigate the sensitivity of the e^+e^- invariant-mass distribution to the hyperon charge radius. We now calculate the $m_{e^+e^-}$ distribution in the range of $m^2_{e^+e^-} < 0.1\,\text{GeV}^2$ with $m_{\Sigma^+\bar{\Sigma}^-} > 2.8\,\text{GeV}$ for the decay $\psi(2S) \to \Sigma^+\bar{\Sigma}^-e^+e^-$ ($m_{\Xi^-\bar{\Xi}^+} > 2.9\,\text{GeV}$ for the decay $\psi(2S) \to \Xi^-\bar{\Xi}^+e^+e^-$) using a dipole EMFF as input. Specifically, we utilize the simple dipole form for G_E in conjunction with the Kelly description [43] for G_M.

In a full experimental analysis, both the type-X contribution can be accounted for by a partial wave analysis similar to that performed in Ref. [32]. Here, to be concrete, we construct the type-X amplitude to get the signal amplitude of Eq. (3). Prior experimental studies indicate that the type-X contribution in the suggested kinematic region is saturated by four charmonia: η_c, χ_{c0}, χ_{c1} and χ_{c2} [44]. Transitions among the initial $\psi(2S)$ and these X charmonia are consistently parameterized with two couplings: one for η_c and the other for the three χ_{cJ} states, which is facilitated by an effective Lagrangian grounded in heavy quark spin symmetry [45,46]. Moreover, a phenomenological transition form factor $f_\psi(q^2) = 1/(1 - q^2/\Lambda_X^2)$ with $\Lambda_X = m_\omega$ is introduced, which has been widely used in analyzing the J/ψ Dalitz decay [47–49]. Subsequent decays of $X \to Y\bar{Y}$ are described within the orbital-spin partial-wave framework [33,35], similar to that of $\psi(2S) \to Y\bar{Y}$ vertices. All the effective couplings are determined by the relevant partial widths listed in the Review of Particle Physics (RPP) [20]. Technical details can be found in the Supplemental Material [42].

First, we estimate the expected event yields for the radii extractions of the Σ^+ and Ξ^- from the $\psi(2S)$ data sets at BESIII and STCF by integrating the differential decay rate given in Eq. (1) over the relevant kinematic region of interest. It is found that there would be around $\mathcal{O}(10^2)$ events for both the Σ^+ and Ξ^- cases at BESIII, and about 300 times more for both cases at STCF. To better investigate the sensitivity to charge radii of Σ^+ and Ξ^-, we generate synthetic data following the distribution of the dipole form factor (for simplicity) for the Σ^+ and Ξ^- with $r_E^{\Sigma^+} = r_E^{\Xi^-} = 0.80$ fm using the von Neumann rejection method. We generate two sets of samples with 2×10^2 and 2×10^4 events, corresponding to simulations of the BESIII [50] and STCF [31] experiments. Fitting to the synthetic data leads to 1.02(23) fm for Σ^+ and 1.13(23) fm for Ξ^- in the context of the BESIII experiment, see Fig. 4. Results for the STCF experiment are presented in Fig. 5, yielding 0.78(4) fm for Σ^+ and 0.80(3) fm for Ξ^-. Notice that the point-like ansatz for Σ^+ and Ξ^- is used as a reference in Fig. 4 and Fig. 5. Consequently, effects from sources other than the elastic EMFFs of hyperons get largely neutralized. The reduced invariant mass distribution of e^+e^- exhibits a kink behavior at the right endpoints of the three χ_{cJ} resonances when projected onto the $m_{e^+e^-}$ axis, attributed to their narrow widths.

We also test the robustness of the simulation results by conservatively varying the involved parameter values, which can be fixed in a real analysis of the experimental data. The gray bands in Fig. 4 and Fig. 5 count the effects of amplitude parameters to the radii extractions, which are obtained by varying the S/D ratio of the $\psi(2S)Y\bar{Y}$ vertex by 20% (the uncertainty as determined in Ref. [34] is only 2%), varying the charmonium transition couplings by 15% and Λ_X in the transition form factors $f_\psi(q^2)$ by 0.2 GeV. That the gray bands are within the 1σ region of the optimal charge radii suggests that the charge radius of Σ^+

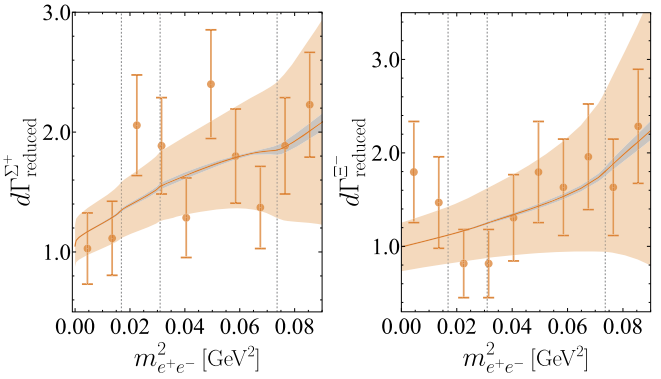

Fig. 4. Fit to 200 synthetic Monte Carlo events using 0.8 fm as the input radius value: Σ^+ (left) and Ξ^- (right). The extracted radii from fitting to the two data sets are 1.02(23) fm for Σ^+ and 1.13(23) fm for Ξ^-, respectively. Three vertical dashed lines denote the right endpoints of the three χ_{cJ} resonances (from left to right: χ_{c2}, χ_{c1} and χ_{c0}) projected onto the $m_{e^+e^-}$ axis. The gray bands show the effects of model parameters to the radii extractions, as detailed in the text.

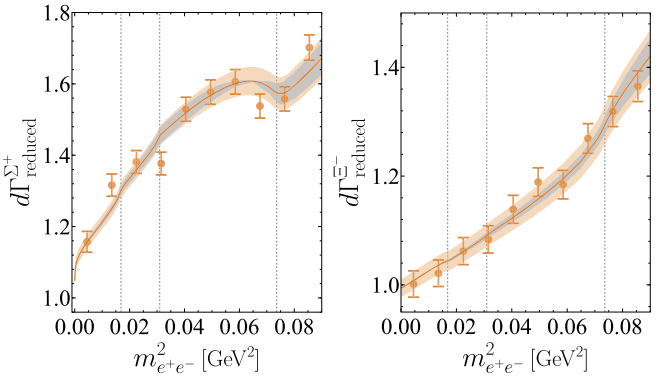

Fig. 5. Fit to 2×10^4 synthetic Monte Carlo events using 0.8 fm as the input radius value: Σ^+ (left) and Ξ^- (right). The extracted radii from fitting to the two data sets are 0.78(4) fm for Σ^+ and 0.80(3) fm for Ξ^-, respectively. For notations, refer to Fig. 4.

or Ξ^- predominates over these amplitude parameters in dictating the e^+e^- invariant-mass distribution in the low $m_{e^+e^-}$ region, given the current experimental precision. As event counts increase, a combined fit incorporating all amplitude parameters and the charge radius becomes essential for a precise radius extraction using the proposed methodology.

This novel approach may also be checked by extracting the proton charge radius from the analogous Dalitz decay $J/\psi \to p\bar{p}e^+e^-$ at the BESIII and STCF experiments; details of the applicability study can be found in the Supplemental Material [42].

4. Summary and prospect

In this Letter, we propose to measure the charge radii of charge hyperons Σ^+ and Ξ^- from the time-like region of the Dalitz decays $\psi(2S) \to Y\bar{Y}e^+e^-$. The $-Q^2$ value can reach $\sim 4m_e^2 = 1.05\times10^{-6}$ GeV^2, which is unprecedentedly low even for the proton charge radius measurements, making use of the advantage that the electron and positron with transverse momenta can be detected with very efficiency.

The optimal kinematic region for extracting the elastic EMFFs of Σ^+ and Ξ^- is identified to be $m_{\Sigma^+\bar{\Sigma}^-} > 2.8$ GeV for the decay $\psi(2S) \to \Sigma^+\bar{\Sigma}^-e^+e^-$ and $m_{\Xi^-\bar{\Xi}^+} > 2.9$ GeV for the decay $\psi(2S) \to \Xi^-\bar{\Xi}^+e^+e^-$, where the involved photon-baryon coupling is dominated by the elastic EMFFs of Σ^+ and Ξ^- and a clean background subtraction can in principle be performed. The latter is achievable through measuring the decays into neutral hyperons $\psi(2S) \to \Sigma^0\bar{\Sigma}^0e^+e^-$ and $\psi(2S) \to \Xi^0\bar{\Xi}^0e^+e^-$ and subtracting their event distributions from those of $\psi(2S) \to \Sigma^+\bar{\Sigma}^-e^+e^-$ and $\psi(2S) \to \Xi^-\bar{\Xi}^+e^+e^-$, respectively.

From a Monte Carlo simulation, we find that already with the BESIII data sample of $\psi(2S)$, the charge radii of the Σ^+ and Ξ^- can be extracted with an uncertainty of 20% level. The precision can be significantly improved with two orders of magnitude more events at STCF. First measurements of the charge radii of Σ^+ and Ξ^-, which have not been achieved so far, are foreseen employing this novel approach.

Declaration of competing interest

The authors declare that they have no known competing financial interests or personal relationships that could have appeared to influence the work reported in this paper.

Data availability

Data will be made available on request.

Acknowledgements

We are grateful to Hai-Bo Li, Jian-Ping Ma, Wei-Zhi Xiong, Hai-Qing Zhou and Xiao-Rong Zhou for useful discussions. YHL and UGM are grateful to the hospitality of the Institute of Theoretical Physics, Chinese Academy of Sciences (CAS), where part of the work was done. This work is supported in part by the CAS under Grants No. YSBR-101 and No. XDB34030000; by the National Natural Science Foundation of China (NSFC) and the Deutsche Forschungsgemeinschaft (DFG) through the funds provided to the Sino-German Collaborative Research Center TRR110 "Symmetries and the Emergence of Structure in QCD" (NSFC Grant No. 12070131001, DFG Project-ID 196253076); by the NSFC under Grants No. 12125507, No. 11835015, and No. 12047503; by CAS through the President's International Fellowship Initiative (PIFI) under Grant No. 2025PD0022; and by the VolkswagenStiftung under Grant No. 93562.

Appendix A. Supplementary material

Supplementary material related to this article can be found online at https://doi.org/10.1016/j.physletb.2024.138887.

References

[1] V. Punjabi, C.F. Perdrisat, M.K. Jones, E.J. Brash, C.E. Carlson, The structure of the nucleon: elastic electromagnetic form factors, Eur. Phys. J. A 51 (2015) 79, arXiv:1503.01452 [nucl-ex].
[2] T. Horn, C.D. Roberts, The pion: an enigma within the Standard Model, J. Phys. G 43 (2016) 073001, arXiv:1602.04016 [nucl-th].
[3] G. Ramalho, M.T. Peña, Electromagnetic transition form factors of baryon resonances, Prog. Part. Nucl. Phys. 136 (2024) 104097, arXiv:2306.13900 [hep-ph].
[4] R. Pohl, et al., The size of the proton, Nature 466 (2010) 213.
[5] A. Antognini, et al., Proton structure from the measurement of $2S$–$2P$ transition frequencies of muonic hydrogen, Science 339 (2013) 417.
[6] P.J. Mohr, B.N. Taylor, D.B. Newell, CODATA recommended values of the fundamental physical constants, Rev. Mod. Phys. 80 (2006) 633, arXiv:0801.0028 [physics.atom-ph], 2008.
[7] Y.-H. Lin, H.-W. Hammer, U.-G. Meißner, New insights into the nucleon's electromagnetic structure, Phys. Rev. Lett. 128 (2022) 052002, arXiv:2109.12961 [hep-ph].
[8] E. Tiesinga, P.J. Mohr, D.B. Newell, B.N. Taylor, CODATA recommended values of the fundamental physical constants: 2018, Rev. Mod. Phys. 93 (2021) 025010.
[9] G. Höhler, E. Pietarinen, Electromagnetic radii of nucleon and pion, Phys. Lett. B 53 (1975) 471.
[10] M. Hoferichter, B. Kubis, J. Ruiz de Elvira, H.W. Hammer, U.-G. Meißner, On the $\pi\pi$ continuum in the nucleon form factors and the proton radius puzzle, Eur. Phys. J. A 52 (2016) 331, arXiv:1609.06722 [hep-ph].
[11] H.-W. Hammer, U.-G. Meißner, The proton radius: from a puzzle to precision, Sci. Bull. 65 (2020) 257, arXiv:1912.03881 [hep-ph].
[12] J.-P. Karr, D. Marchand, E. Voutier, The proton size, Nat. Rev. Phys. 2 (2020) 601.
[13] H. Gao, M. Vanderhaeghen, The proton charge radius, Rev. Mod. Phys. 94 (2022) 015002, arXiv:2105.00571 [hep-ph].

[14] Y.-H. Lin, H.-W. Hammer, U.-G. Meißner, Dispersion-theoretical analysis of the electromagnetic form factors of the nucleon: past, present and future, Eur. Phys. J. A 57 (2021) 255, arXiv:2106.06357 [hep-ph].
[15] C. Peset, A. Pineda, O. Tomalak, The proton radius (puzzle?) and its relatives, Prog. Part. Nucl. Phys. 121 (2021) 103901, arXiv:2106.00695 [hep-ph].
[16] A. Antognini, F. Hagelstein, V. Pascalutsa, The proton structure in and out of muonic hydrogen, Annu. Rev. Nucl. Part. Sci. 72 (2022) 389, arXiv:2205.10076 [nucl-th].
[17] W. Xiong, et al., A small proton charge radius from an electron–proton scattering experiment, Nature 575 (2019) 147.
[18] A. Gasparian, et al., PRad, PRad-II: a new upgraded high precision measurement of the proton charge radius, arXiv:2009.10510 [nucl-ex], 2020.
[19] I. Eschrich, et al., SELEX, Measurement of the Σ^- charge radius by Σ^--electron elastic scattering, Phys. Lett. B 522 (2001) 233, arXiv:hep-ex/0106053.
[20] R.L. Workman, et al., Particle Data Group, Review of Particle Physics, PTEP 2022 (2022) 083C01.
[21] V. Bernard, U.-G. Meißner, Electromagnetic structure of the pion and the kaon, Phys. Rev. Lett. 61 (1988) 2296, Phys. Rev. Lett. 61 (1988) 2973, Erratum.
[22] P. Maris, P.C. Tandy, The pi, K+, and K0 electromagnetic form-factors, Phys. Rev. C 62 (2000) 055204, arXiv:nucl-th/0005015.
[23] G. Wagner, A.J. Buchmann, A. Faessler, Exchange currents in octet hyperon charge radii, Phys. Rev. C 58 (1998) 3666, arXiv:nucl-th/9809015.
[24] B. Kubis, U.-G. Meißner, Baryon form-factors in chiral perturbation theory, Eur. Phys. J. C 18 (2001) 747, arXiv:hep-ph/0010283.
[25] A.N. Hiller Blin, Systematic study of octet-baryon electromagnetic form factors in covariant chiral perturbation theory, Phys. Rev. D 96 (2017) 093008, arXiv:1707.02255 [hep-ph].
[26] M. Yang, P. Wang, Electromagnetic form factors of octet baryons with the nonlocal chiral effective theory, Phys. Rev. D 102 (2020) 056024, arXiv:2005.11971 [hep-ph].
[27] B. Yan, C. Chen, J.-J. Xie, Σ and Ξ electromagnetic form factors in the extended vector meson dominance model, Phys. Rev. D 107 (2023) 076008, arXiv:2301.00976 [hep-ph].
[28] A.A. Filin, V. Baru, E. Epelbaum, H. Krebs, D. Möller, P. Reinert, Extraction of the neutron charge radius from a precision calculation of the deuteron structure radius, Phys. Rev. Lett. 124 (2020) 082501, arXiv:1911.04877 [nucl-th].
[29] D. Chatterjee, I. Vidaña, Do hyperons exist in the interior of neutron stars?, Eur. Phys. J. A 52 (2016) 29, arXiv:1510.06306 [nucl-th].
[30] M. Ablikim, et al., BESIII, Determination of the number of $\psi(3686)$ events taken at BESIII, arXiv:2403.06766 [hep-ex], 2024.
[31] M. Achasov, et al., STCF conceptual design report (Volume I): Physics & Detector, Front. Phys. (Beijing) 19 (2024) 14701, arXiv:2303.15790 [hep-ex].
[32] R. Kappert, Partial-wave analysis of the radiative decay of J/ψ into $p\bar{p}$, Ph.D. thesis, Groningen U, 2022, arXiv:2302.06458 [hep-ex].
[33] B.S. Zou, D.V. Bugg, Covariant tensor formalism for partial wave analyses of ψ decay to mesons, Eur. Phys. J. A 16 (2003) 537, arXiv:hep-ph/0211457.
[34] S.-M. Wu, J.-J. Wu, B.-S. Zou, Effective radius for production of baryon-antibaryon pairs from ψ decays, Phys. Rev. D 104 (2021) 054018, arXiv:2104.09908 [hep-ph].
[35] H.-J. Jing, D. Ben, S.-M. Wu, J.-J. Wu, B.-S. Zou, Covariant orbital-spin scheme for any spin based on irreducible tensor, J. High Energy Phys. 06 (2023) 039, arXiv:2301.01575 [hep-ph].
[36] V. Pascalutsa, M. Vanderhaeghen, S.N. Yang, Electromagnetic excitation of the $\Delta(1232)$-resonance, Phys. Rep. 437 (2007) 125, arXiv:hep-ph/0609004.
[37] L. Tiator, D. Drechsel, S.S. Kamalov, M. Vanderhaeghen, Electromagnetic excitation of nucleon resonances, Eur. Phys. J. Spec. Top. 198 (2011) 141, arXiv:1109.6745 [nucl-th].
[38] J. Guttmann, M. Vanderhaeghen, Theoretical analysis of the $p\bar{p} \to \pi^0 e^+ e^-$ process within a Regge framework, Phys. Lett. B 719 (2013) 136, arXiv:1210.3290 [hep-ph].
[39] F. Gross, D.O. Riska, Current conservation and interaction currents in relativistic meson theories, Phys. Rev. C 36 (1987) 1928.
[40] S. Scherer, A.Y. Korchin, J.H. Koch, Virtual Compton scattering off the nucleon at low-energies, Phys. Rev. C 54 (1996) 904, arXiv:nucl-th/9605030.
[41] H. Haberzettl, K. Nakayama, S. Krewald, Gauge-invariant approach to meson photoproduction including the final-state interaction, Phys. Rev. C 74 (2006) 045202, arXiv:nucl-th/0605059.
[42] See the Supplemental Material for technical details of the hadronic operators, gauge invariance and application to the proton case.
[43] J.J. Kelly, Simple parametrization of nucleon form factors, Phys. Rev. C 70 (2004) 068202.
[44] J.P. Alexander, et al., CLEO, Study of $\psi(2S)$ decays to $\gamma p\bar{p}$, $\pi^0 p\bar{p}$ and $\eta p\bar{p}$ and search for $p\bar{p}$ threshold enhancements, Phys. Rev. D 82 (2010) 092002, arXiv:1007.2886 [hep-ex].
[45] F. De Fazio, Radiative transitions of heavy quarkonium states, Phys. Rev. D 79 (2009) 054015, arXiv:0812.0716 [hep-ph], Phys. Rev. D 83 (2011) 099901, Erratum.
[46] Z.-G. Wang, Analysis of the radiative decays among the charmonium states, Int. J. Theor. Phys. 51 (2012) 1518, arXiv:1101.0474 [hep-ph].
[47] J. Fu, H.-B. Li, X. Qin, M.-Z. Yang, Study of the electromagnetic transitions $J/\psi \to Pl^+l^-$ and probe dark photon, Mod. Phys. Lett. A 27 (2012) 1250223, arXiv:1111.4055 [hep-ph].
[48] M. Ablikim, et al., BESIII, Observation of J/ψ electromagnetic Dalitz decays to $X(1835)$, $X(2120)$ and $X(2370)$, Phys. Rev. Lett. 129 (2022) 022002, arXiv:2112.14369 [hep-ex].
[49] M. Ablikim, et al., BESIII, Observation of the hindered electromagnetic Dalitz decay $\psi(3686) \to e^+ e^- \eta_c$, Phys. Rev. D 106 (2022) 112002, arXiv:2208.12241 [hep-ex].
[50] M. Ablikim, et al., BESIII, Future physics programme of BESIII, Chin. Phys. C 44 (2020) 040001, arXiv:1912.05983 [hep-ex].